Glycoconj J (2008) 25:291–304
DOI 10.1007/s10719-007-9091-7

Glycosphingolipids in vascular endothelial cells: relationship of heterogeneity in Gb3Cer/CD77 receptor expression with differential Shiga toxin 1 cytotoxicity

Christian H. Schweppe · Martina Bielaszewska · Gottfried Pohlentz · Alexander W. Friedrich · Heino Büntemeyer · M. Alexander Schmidt · Kwang S. Kim · Jasna Peter-Katalinić · Helge Karch · Johannes Müthing

Received: 27 August 2007 / Revised: 18 October 2007 / Accepted: 15 November 2007 / Published online: 5 January 2008

Abstract Shiga toxin (Stx) 1 binds to the glycosphingolipid (GSL) globotriaosylceramide (Gb3Cer/CD77) and injures human endothelial cells. In order to gain insight into Stx1-induced cellular impairment, we analysed in detail the molecular heterogeneity of Stx1 receptors in two endothelial cell lines differing in their Stx1-sensitivity. We observed a moderate sensitivity to Stx1 of human brain microvascular endothelial cells (HBMECs, CD_{50}>200 ng/ml), but a considerably higher mortality rate in cultures of EA.hy 926 cells, a cell line derived from human umbilical vein endothelial cells (CD_{50} of 0.2 ng/ml). Immunofluorescence microscopy demonstrated the presence of Gb3Cer in both cell lines, but showed an enhanced content of Gb3Cer in EA.hy 926 cells. Solid phase overlay binding assays of isolated GSLs combined with nanoelectrospray ionization quadrupole time-of-flight mass spectrometry demonstrated a balanced proportion of Gb3Cer and globotetraosylceramide (Gb4Cer) in HBMECs, but an increase of Gb3Cer and absence of Gb4Cer in EA.hy 926 cells. Gb3Cer species with C24:1/C24:0 fatty acids were found to dominate over those with C16:0 fatty acids in EA.hy 926 cells, but were similarly distributed in HBMECs. Reverse transcriptase polymerase chain reaction indicated the concomitant presence of Gb3Cer and Gb4Cer synthases in HBMECs, whereas EA.hy 926 cells expressed Gb3Cer synthase, but completely lacked Gb4Cer synthase. This deficiency, resulting in the accumulation of Gb3Cer in EA.hy 926 cells, represents the most prominent molecular reason that underlies the different Stx1 sensitivities of HBMECs and EA.hy 926 endothelial cells.

Keywords Glycolipids · HBMECs · EA.hy 926 cells · Glycosyltransferases

C. H. Schweppe · M. Bielaszewska · A. W. Friedrich · H. Karch
Institute for Hygiene, University of Münster,
48149 Münster, Germany

C. H. Schweppe · A. W. Friedrich · H. Karch
Interdisciplinary Center for Clinical Research (IZKF) Münster,
48149 Münster, Germany

G. Pohlentz · J. Peter-Katalinić · J. Müthing (✉)
Institute for Medical Physics and Biophysics,
University of Münster,
Robert-Koch-Str. 31,
48149 Münster, Germany
e-mail: jm@uni-muenster.de

H. Büntemeyer
Institute for Cell Culture Technology, University of Bielefeld,
33501 Bielefeld, Germany

M. Alexander Schmidt
Institute of Infectiology, University of Münster,
48149 Münster, Germany

K. S. Kim
Division of Pediatric Infectious Diseases,
Johns Hopkins University School of Medicine,
Baltimore, MD 21287, USA

Abbreviations

CID	Collision-induced-dissociation
DTAF	dichlorotriazinylamino fluorescein
EA.hy 926	HUVEC derived endothelial cell line

ESI Q-TOF-MS	electrospray ionization quadrupole time-of-flight mass spectrometry
GSL(s)	glycosphingolipid(s)
HBMECs	human brain microvascular endothelial cells
HPTLC	high-performance thin-layer chromatography
HUVECs	human umbilical vein endothelial cells
RT-PCR	reverse transcriptase polymerase chain reaction
Stx	Shiga toxin

Introduction

Shiga toxins (Stxs), also referred to as verotoxins, are AB_5 holotoxins, which have been divided into two families, Stx1 and Stx2, each of which consists of the major Stx type and several variants [1, 2]. The B-subunit pentamer of Stx1 binds to its receptor globotriaosylceramide (Gb3Cer/CD77) [3] on the surface of susceptible endothelial cells [4]. Stxs are internalized and undergo retrograde transport through the Golgi apparatus to the endoplasmic reticulum [5]. After translocation into the cytosol, the A-subunit is cleaved into an enzymatically active A1 fragment (27.5 kDa) and a small A2 fragment (4.5 kDa). The A1 fragment possesses the rRNA *N*-glycosidase activity [6] and depurinates an adenosine at position 4324 of the 28S ribosomal RNA causing death of the target cell through inhibition of protein synthesis [7].

Glycosphingolipids (GSLs), amphipathic molecules composed of a hydrophilic oligosaccharide chain and a hydrophobic ceramide part [8, 9], are located primarily in the outer leaflet of the plasma membrane of animal cells. Their oligosaccharide chains spread in the aqueous environment at the cell surface, and this makes them excellent candidates for cell surface recognition molecules [10–12]. Consequently, GSLs play important biological roles in the pathophysiology of many infections and serve as receptors for bacteria [13–15] and bacterial toxins including Stxs [4, 16].

To gain insight into the Stx1-mediated impairment of the vascular endothelium, we used human brain microvascular endothelial cells (HBMECs) [17] and EA.hy 926 cells, a cell line derived by fusing human umbilical vein endothelial cells (HUVECs) to the human lung epithelial cell line A549 [18]. HBMECs, which form the barrier that protects the brain from microbes and toxins circulating in the blood [19, 20], have been employed in numerous studies as target cells for pathogen invasion [21, 22], fimbriae-mediated bacterial interactions [23], and bacterial toxins [24, 25]. EA.hy 926 cells, which represent "immortalized" HUVECs [26], have been proved to be a reliable model for *in vitro* studies of certain aspects of angiogenesis [27, 28], vascular inflammation [29], and toxin-mediated cell cycle arrest [24].

Binding of Stx to Gb3Cer on endothelial cells is postulated to be the critical event triggering the vascular injury caused by Stx-producing *Escherichia coli* [2, 20]. Though the importance of GSLs as receptors for Stxs is well documented [4], the GSL composition of endothelial cells has generally received low attention. In the best characterized HUVECs [30, 31], globo-series neutral GSLs were the major GSLs [32, 33] as in primary human brain microvascular endothelial cells [34]. Upon stimulation with inflammatory mediators, an enhanced expression of Gb3Cer has been reported for HUVECs [35] and primary human brain endothelial cells from various sources [36–39].

Although the HBMECs, established by Kim and colleagues [17], and EA.hy 926 cells [18] have been extensively studied, no information is available about their GSLs. In this study, the molecular basis for the differential cytotoxic action of Stx1 on HBMECs and EA.hy 926 cells was investigated. Initially, we started with the immunofluorescence microscopic investigation of the globo-series GSLs Gb3Cer and globotetraosylceramide (Gb4Cer), whereby Gb4Cer represents the elongation structure of Gb3Cer synthesized by β1,3-*N*-acetylgalactosaminyltransferase. We then explored Stx1-mediated cytotoxicity in both cell lines. To gain insights into the molecular structures responsible for the differences in Stx1 susceptibility, we examined the expression of receptor-relevant glycosyltransferases by means of reverse transcriptase polymerase chain reaction, and the GSL profiles and Gb3Cer content by solid phase binding assays. Finally, the Stx1-binding Gb3Cer species were further structurally characterized by mass spectrometry. Our findings provide an understanding of the basis of increased sensitivity of the HUVEC-derived EA.hy 926 cell line to Stx1, which has not been reported before.

Materials and methods

Cell cultures

HBMECs [17] and HUVEC-derived EA.hy 926 cells [18] were maintained as described previously [24]. For large scale production, cells were propagated on collagen precoated Cytodex 3 microcarriers (Amersham Biosciences AB, Uppsala, Sweden) in spinner vessels [33, 40]. Briefly, inocula for 1 l volumes were prepared using the 30th passage of HBMECs and the 13th passage of EA.hy 926 cells in 200 ml spinner cultures containing 3 g/l of Cytodex 3 microcarriers. Scale-up was performed in a 1 l membrane stirred SuperSpinner [41]. The beads covered with endothelial cells were washed twice with phosphate buffered saline (PBS) before extraction of GSLs.

Preparation of GSL extracts from endothelial cells

Endothelial cells were extracted with methanol, chloroform/methanol (1/2, v/v), chloroform/methanol (1/1, v/v), and chloroform/methanol (2/1, v/v). The combined extracts of HBMECs and EA.hy 926 cells, respectively, were dried and phospholipids were saponified with aqueous 1 M NaOH for 1 h at 37°C. After neutralization with 10 M HCl, the samples were dialyzed against deionized water and dried. The extracts were adjusted to defined volumes of chloroform/methanol (2/1, v/v) corresponding to 1×10^5 cells/µl.

Purification of Stx1

Stx1 was purified as described previously [42] from *E. coli* C600 strain lysogenised with bacteriophage H19J (*E. coli* C600(H19J)) which encodes Stx1. Briefly, Stx1 was eluted from agar plates exhibiting confluent lysis after inoculation with the bacteriophage, precipitated with 50% ammonium sulfate, applied to a Sepharyl S200 column, and fractions with cytotoxic activity in the molecular range between 30 and 80 kDa were concentrated. Stx1 was further purified by an Affi-Gel Blue column, chromatofocusing and high performance liquid chromatography. Purity of the Stx1 preparation was monitored by SDS-PAGE.

Cytotoxicity and cell viability

Direct measurement of Stx1 cytotoxicity was performed in 96-well plates (Corning Inc., Corning, NY, USA) seeded with 1×10^4/well of HBMECs or 3×10^4/well of EA.hy 926 cells. After overnight incubation, 100 µl of 10-fold dilutions of Stx1 preparation in cell culture medium (starting concentration of 200 ng/ml) or 100 µl of the medium as a control were added to the confluent cell monolayers in triplicate and incubated for 3 days at 37°C in a 5% CO_2-air atmosphere. The cells were then fixed with 70% ethanol, stained with 10% Giemsa and examined microscopically for cytotoxicity. The toxin concentration, which caused a cytotoxic effect in 50% of the cells was defined as a 50% cytotoxic dose (CD_{50}).

The reduction of 4-[3-(4-iodophenyl)-2-(4-nitrophenyl)-2H-5-tetrazolio]-1,3-benzene disulfonate (WST-1; Roche Diagnostics GmbH, Penzberg, Germany) to formazan served as an indirect measurement of cell viability. The WST-1 assay was performed as described previously [24], with minor modifications. Briefly, after overnight incubation the cells grown in 96-well plates were exposed to 10-fold dilutions of Stx1 preparation (concentrations as above) and incubated for 54 h. Ten µl of WST-1 solution (5 mg/ml in PBS) were added to each well, incubated for 3 h at 37°C, and 100 µl of lysis buffer (20% (w/v) SDS in 50% *N*,*N*-dimethyl formamide, pH 4.7) were added to the cells overnight. The absorbance was measured at 450 nm with a microplate reader (OpsysMR absorbance reader, equipped with software revelation 4.21; Dynex Technologies, Worthing, West Sussex, UK).

Anti-GSL antibodies and anti-Stx1 antibodies

All polyclonal rabbit and chicken antibodies were generated according to the method of Kasai *et al.* [43]. The preparation and specificities of the antibodies against various neutral GSLs and gangliosides have been reported in previous publications [44, 45], and the related references are listed in Table 1. Stx1 was detected with the mouse IgG1 monoclonal antibody 109/4-E9b (Sifin, Berlin, Germany).

Immunofluorescence microscopy

HBMECs and EA.hy 926 cells were seeded in 4-well polystyrene chamber slides (Tissue culture chambers,

Table 1 Monoclonal and polyclonal antibodies employed for the identification and structural characterization of GSLs from HBMECs and EA.hy 926 cells

Name	Structure	References[a]
Lc2Cer	Galβ1-4Glcβ1-1Cer	[33, 40]
Gb3Cer	Galα1-4Galβ1-4Glcβ1-1Cer	[33, 40, 42, 72]
Gb4Cer	GalNAcβ1-3Galα1-4Galβ1-4Glcβ1-1Cer	[33, 42, 72]
Gg3Cer	GalNAcβ1-4Galβ1-4Glcβ1-1Cer	[33, 40, 50]
Gg4Cer	Galß1-3GalNAcβ1-4Galβ1-4Glcβ1-1Cer	[33, 40, 72, 73]
nLc4Cer	Galβ1-4GlcNAcβ1-3Galβ1-4Glcβ1-1Cer	[33, 40, 49, 72]
GM3	Neu5Acα2-3Galβ1-4Glcβ1-1Cer	[33, 40, 72, 74]
GM2	GalNAcβ1-4(Neu5Acα2-3)Galβ1-4Glcβ1-1Cer	[72, 74]

All antibodies are polyclonal chicken IgY antibodies with the exception of anti-Gg3Cer (2D4, mouse monoclonal IgM) and anti-Gg4Cer antibody (rabbit polyclonal IgG).

[a] References concerning the antibodies used in this study.

The nomenclature of the GSLs follows the IUPAC-IUB recommendations 1997 [75].

Permanox®, no. 177437; Nunc GmbH, Wiesbaden-Biebrich, Germany) in amounts of 1.5×10^4 and 2×10^4 cells/chamber, respectively, and grown for 48 h until subconfluence. Immunohistochemistry with primary chicken anti-GSL antibodies and secondary dichlorotriazinylamino fluorescein (DTAF) labeled rabbit anti-chicken IgY antibodies (Dianova, Hamburg, Germany) was performed following published protocols [33, 40]. The detection of the Stx1 binding was performed by consecutive incubations of the cells with Stx1 (0.2 μg/ml in 3% bovine serum albumin (BSA) in PBS), monoclonal mouse IgG1 anti-Stx1 antibody 109/4-E9b (2 μg/ml in 3% BSA in PBS), secondary DTAF-labeled goat anti-mouse IgG antibody (1:40) (Dianova) and 4′,6-diamidine-2-phenylindole-dihydrochloride (DAPI) solution according to the protocol for anti-GSL antibodies [33, 40]. Negative controls without anti-GSL antibodies and Stx1 were processed in parallel.

The cell monolayers were embedded in 20% Mowiol (Calbiochem, Darmstadt, Germany) and bound DTAF-labeled antibodies as well as stained nuclei were visualized under fluorescence microscope (Axiophot, Zeiss, Göttingen, Germany), original magnification ×400 (objective lens Plan-NEOFLUAR, numerical aperture 0.75), with filter sets adequate to the maxima of absorption/emission of DTAF (495/528 nm) and of DAPI (368/488 nm). The fluorescence was recorded with an AxioCam CCD camera (Zeiss), documented with AxioVision 3.1 (Zeiss, 1,300×1,030 pixel) and processed with Adobe Photoshop software (Adobe Systems Inc.).

Reverse transcriptase polymerase chain reaction (RT-PCR) for glycosyltransferases

Total cellular RNA was isolated from 1×10^6 endothelial cell aliquots using the RNeasy Mini kit (Qiagen, Hilden, Germany; no. 74106) according to the supplier's protocol and transcribed by moloney murine leukemia virus (M-MLV) reverse transcriptase. First-strand cDNA synthesis was performed using the SuperScriptTM II RT kit (Invitrogen, Karlsruhe, Germany; no. 18064-014). Primers were synthesized by Operon Biotechnologies, Inc. (Köln, Germany). The primers used were as follows: β1,4-galactosyltransferase (β1,4-GalT, EC 2.4.1.-; GenBank accession no. AF097159), sense 5′-AACGGTACAGATTATCCCGAAGG-3′, antisense 5′-TGGAGCTAACTCTGGCATGAGG-3′ [38]; α1,4-galactosyltransferase (α1,4-GalT, EC 2.4.1.228; GenBank accession no. AJ245581), sense 5′-ATGTCCAAGCCCCCCGACCTC-3′, antisense 5′-GAGCTGCCCTTTCTCCTTGGG-3′ [46]; β1,3-*N*-acetylgalactosaminyltransferase (β1,3-GalNAcT, EC 2.4.1.79; GenBank accession no. Y15062), sense 5′-ATGGCCTCGGCTCTCTGGACT-3′, antisense 5′-TTGTAGTGGGGAAGGCTGAGGT-3′. The primers were designed with the Oligonucleotide Properties Calculator freeware (http://www.basic.northwestern.edu/biotools/oligocalc.html). An aliquot of 2.5 μl of the cDNA preparation was added to the PCR mixture containing 2.5 μl of 10-fold-concentrated polymerase synthesis buffer Y, 0.75 μl $MgCl_2$ (25 mM), 5 μl of enhancer solution, 0.5 μl dNTP mix (10 mM each), 0.5 μl (100 mM) of each primer and 0.4 μl (2 U) of *Taq* DNA polymerase (all reagents from Peqlab, SAWADY kit no. 01-1040) and filled up with distilled water to a final volume of 25 μl. After DNA denaturing at 94°C for 3 min 30 s, PCR was performed in 30 cycles of 94°C for 15 s, 62°C (β1,4-GalT) or 64°C (α1,4-GalT and β1,3-GalNAcT) for 30 s, 72°C for 1 min, with a final extension at 72°C for 10 min.

Forty percent aliquots from total RNA after RT-PCRs were subjected to electrophoresis in 1% agarose gels, followed by photographic recording of the ethidium bromide stained gels. Fluorescence was measured using a Fluor-Imager ChemiDoc® XRS (Bio-Rad, München, Germany) and documented with Quantity One 4.5.1 (Bio-Rad) and Photoshop software (Adobe).

Reference GSLs

A mixture of neutral GSLs, comprising monohexosylceramide (MHC), lactosylceramide (Lc2Cer), Gb3Cer, and Gb4Cer, was prepared from human erythrocytes. Neutral GSL references of neolacto- and ganglio-series were from human granulocytes and murine MDAY-D2 cell line, respectively [47]. A ganglioside mixture containing GM3 was isolated from human granulocytes as described [48]. Abbreviations and corresponding structures of GSLs used in this study are depicted in Table 1.

High-performance thin-layer chromatograhy (HPTLC)

GSLs were separated on glass-backed silica gel 60 precoated HPTLC-plates (no. 5633; Merck, Darmstadt, Germany) in the solvent chloroform/methanol/water (120/70/17, each by vol., with 2 mM $CaCl_2$). Orcinol- and immunostained GSL bands (see "HPTLC immunostaining") were scanned with a CD60 scanner (Desaga, Heidelberg, Germany, software ProQuant^R, version 1.06.000). Bands were quantified in reflectance mode at 544 nm (orcinol) and 630 nm (indolylphosphate) with a light beam slit of 0.1×2 mm.

HPTLC immunostaining

The HPTLC immunodetection procedure using anti-GSL antibodies and Gb3Cer-binding Stx1 in conjunction with anti-Stx1 antibody was employed as previously described [33, 42, 49]. All primary anti-GSL and alkaline phosphatase-labeled secondary antibodies (Dianova) were used in 1:2000 dilutions. Stx1-mediated detection of Gb3Cer was performed

with the anti-Stx1 monoclonal antibody 109/4-E9b (Sifin). Bound secondary antibodies were visualized by color development using 5-bromo-4-chloro-3-indolyl phosphate *p*-toluidine salt (BCIP; Biomol, Hamburg, Germany).

Extraction of GSLs from HPTLC plates

The silica gel of anti-Gb3Cer, anti-Gb4Cer and Stx1-detected GSL bands corresponding to 6×10^6 cells was extracted with chloroform/methanol/water (30/60/8, each by vol.) under sonication [50]. The supernatants from threefold extractions were pooled, dried, redissolved in methanol and analyzed by mass spectrometry without further purification.

NanoElectrospray ionization quadrupole time-of-flight mass spectrometry (nanoESI Q-TOF-MS)

The extracted GSL samples were analyzed in positive ion mode by nanoESI Q-TOF-MS and low-energy collision-induced-dissociation (CID) MS/MS using a Q-TOF mass spectrometer (Micromass, Manchester, U.K.). After selecting the precursor ions of interest with the first quadrupole, CID was performed to obtain fragment ions enabling sequence analysis (for further details see [50, 51]). The nomenclature introduced by Domon and Costello [52, 53] was used for the assignment of the fragment ions.

Results

Immunohistochemical detection of GSLs in HBMECs and EA.hy 926 cells

In order to determine the expression of lactosylceramide (Lc2Cer, the precursor of Gb3Cer) and the globo-series GSLs Gb3Cer and Gb4Cer (for structures see Table 1), anti-GSL antibodies were used for immunofluorescence microscopy of subconfluent HBMEC and EA.hy 926 cell monolayers in parallel with the corresponding nuclear stains. As shown in Fig. 1, anti-Lc2Cer, anti-Gb3Cer, and anti-Gb4Cer as well as the Stx1 immunostains demonstrated moderate positive reactions in HBMECs. In contrast, anti-Lc2Cer and anti-Gb3Cer as well as Stx1 immunostains showed strong positive reactions in EA.hy 926 cells, whereas the anti-Gb4Cer antibody gave a substantially lower signal with these cells (Fig. 2) compared to HBMECs (see Fig. 1). However, the Stx1 immunofluorescence stains demonstrated a moderate and a high fluorescence intensity in HBMECs and EA.hy 926 cells, respectively, consistent with the different intensities of the anti-Gb3Cer staining in these cell types. In all cases, parallel control cultures, incubated with the secondary DTAF-labeled antibodies only, did not stain. These results suggest an accumulation of Lc2Cer and Gb3Cer along with the lack of Gb4Cer in EA.hy 926 cells.

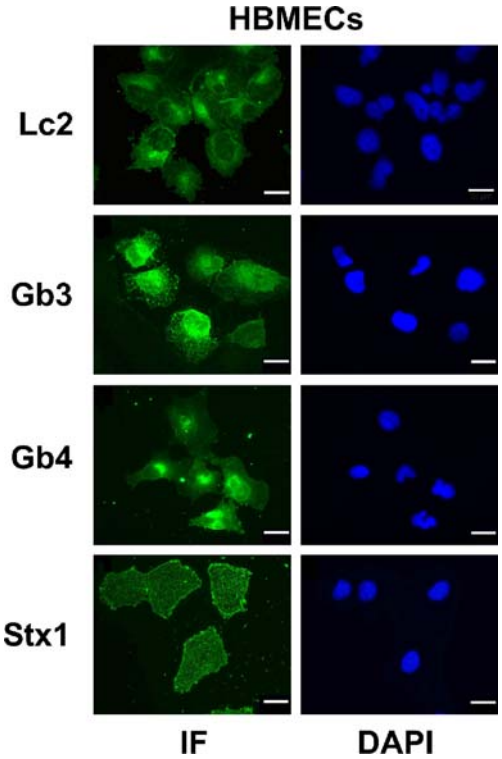

Fig. 1 Detection of neutral GSLs on HBMECs using indirect immunofluorescence microscopy. Detection was performed with anti-Lc2Cer (Lc2), anti-Gb3Cer (Gb3), and anti-Gb4Cer antibodies (Gb4), followed by incubation with DTAF-labeled secondary antibody. Gb3Cer-bound Stx1 was detected with anti-Stx1 and DTAF-labeled secondary antibody. Cell nuclei were stained with DAPI. *Bars* represent 20 µm. IF: immunofluorescence microscopy. The GSL structures are depicted in Table 1

Stx1-mediated cytotoxicity and reduced cell viability

To determine the impact of different Stx1 receptor quantities in HBMECs and EA.hy 926 cells on the cytotoxic potential of Stx1, serial dilutions of the toxin (from 200 ng/ml to 0.2 pg/ml) were incubated with confluent monolayers grown in 96-well microtitre plates. HBMECs were refractory to the cytotoxic action of Stx1, with a CD_{50} > 200 ng/ml. In contrast, EA.hy 926 cells exhibited > 10^3-fold higher sensitivity to Stx1 (CD_{50} of 0.2 ng/ml). Cell viability (Fig. 3) declined after Stx1-treatment in both lines. The mortality rate was considerably increased in EA.hy 926 cell cultures as compared to HBMECs (*ca.* 40 *versus* 80% viable cells, respectively) over concentrations ranging from 0.2 to 200 ng/ml. The concentrations of Stx1 required for 50% reduction of the cell viability were 0.2 ng/ml in EA.hy 926 cells and > 200 ng/ml in HBMECs. These results were in agreement

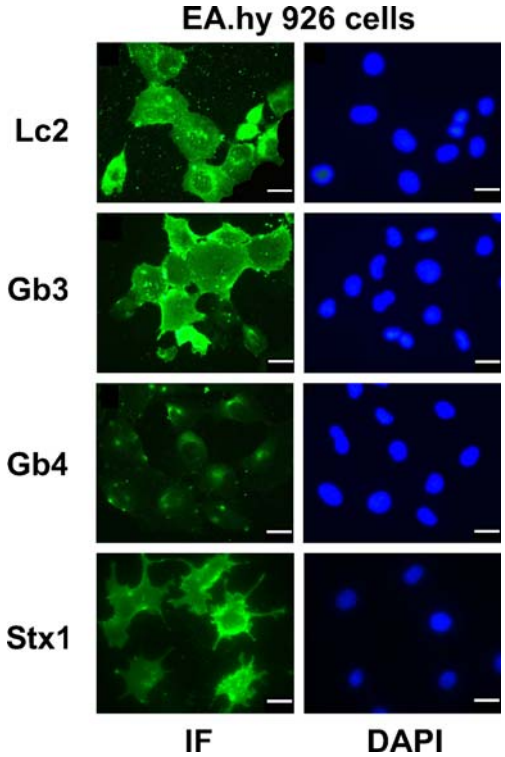

Fig. 2 Detection of neutral GSLs on EA.hy 926 cells using indirect immunofluorescence microscopy. Detection was performed as described in the legend to Fig. 1. *Bars* represent 20 µm. IF: immunofluorescence microscopy. The GSL structures are depicted in Table 1

with the direct cytotoxicity measurements and pointed at the higher concentration of Gb3Cer as the molecular basis for the more pronounced sensitivity of EA.hy 926 cells to Stx1.

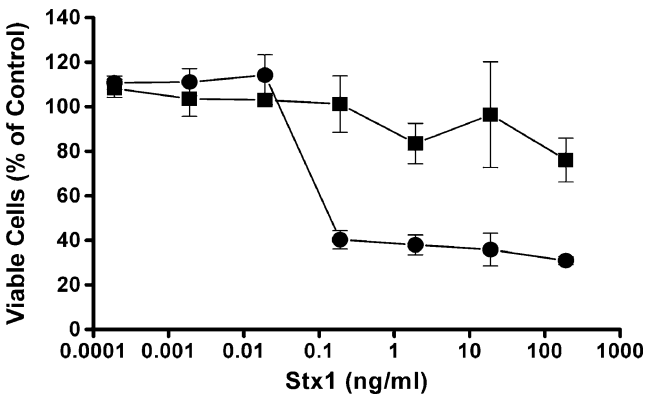

Fig. 3 Stx1-induced decline in cell viability of HBMECs and EA.hy 926 cells determined by cell viability assay. Microtitre plate grown HBMECs (*filled square*) and EA.hy 926 cells (*filled circle*) were treated for 54 h at 37°C with Stx1 concentrations as indicated. Cell viability was determined using the WST-1-assay. Results represent the mean and standard deviation of triplicate determinations and are expressed as a percentage of untreated control cells

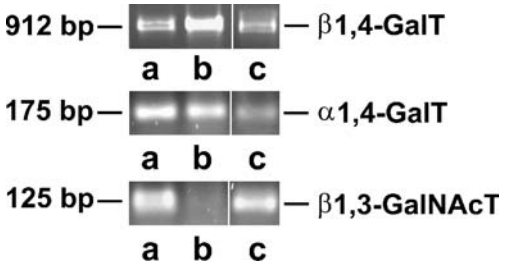

Fig. 4 Glycosyltransferases RNA expression in HBMECs and EA.hy 926 cells. Depicted are electrophoretically separated ethidium bromide-stained PCR amplicons of glycosyltransferases target sequences. Total RNA was assayed for the presence of Lc2Cer synthase (β1,4-GalT), Gb3Cer synthase (α1,4-GalT), and Gb4Cer synthase (β1,3-GalNAcT) using specific RT-PCR primers for the respective glycosyltransferases. **a** HBMECs. **b** EA.hy 926 cells. **c** HUVECs as a control. The *vertical white lines* indicate areas of noncontiguous lanes assembled

RT-PCR analysis of glycosyltransferases in HBMECs and EA.hy 926 cells

To characterize the reasons of the differential GSL expression, HBMECs and EA.hy 926 cells (Fig. 4a and b, respectively) were assayed for β1,4-GalT (Lc2Cer synthase), α1,4-GalT (Gb3Cer synthase), and β1,3-GalNAcT (Gb4Cer synthase) by RT-PCR. HUVECs, well known to express Lc2Cer, Gb3Cer, and Gb4Cer [33], served as a positive control (Fig. 4c) yielding amplicons of 912 bp (β1,4-GalT), 175 bp (α1,4-GalT), and 125 bp (β1,3-GalNAcT). The RT-PCR analyses of HUVECs' glycosyltransferases reflect the cellular GSL profile with clear evidence of Gb4Cer as the predominant GSL in these cells [33]. The concomitant expression of Gb3Cer and Gb4Cer synthases in HBMECs (Fig. 4a) is in agreement with the presence of both GSLs as detected by immunofluorescence microscopy. The most prominent difference between HBMECs and EA.hy 926 cells was the lack of the β1,3-GalNAcT transcript (Gb4Cer synthase) in EA.hy 926 cells (Fig. 4b), consistent with the extremely weak detection of Gb4Cer by immunofluorescence (see Fig. 2). The results suggest that the absence of Gb4Cer, attributed to the lack of β1,3-GalNAcT (Gb4Cer synthase), leads to enhancement of Gb3Cer in EA.hy 926 cells.

Structural characterization of GSLs in HBMECs and EA.hy 926 cells by HPTLC immunodetection

To verify the preliminary evidence for a different content of GSLs, especially an elevated concentration of Gb3Cer and lack of Gb4Cer in EA.hy 926 cells, GSLs were isolated from both cell lines and structurally characterized by HPTLC analysis. Figure 5a shows the orcinol staining of total GSL extracts from HBMECs and EA.hy 926 cells compared to reference neutral GSLs from human eryth-

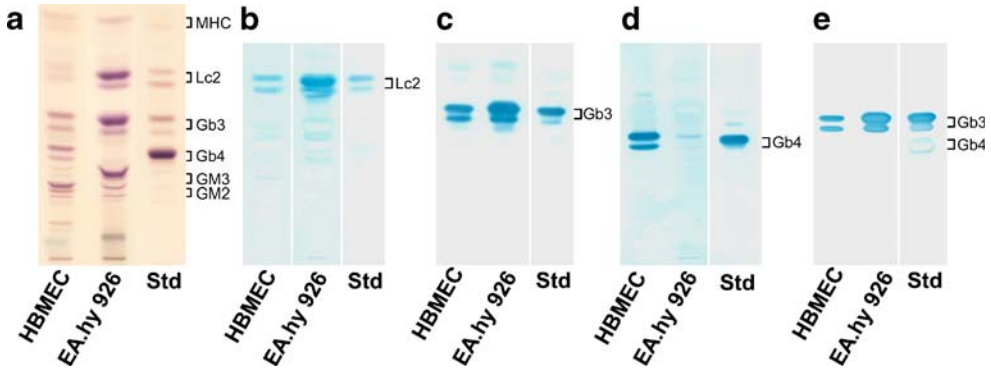

Fig. 5 HPTLC immunodetection of neutral GSLs in lipid extracts from HBMECs and EA.hy 926 cells. **a** Orcinol stain of HPTLC-separated GSLs; corresponding HPTLC overlay assays with **b** anti-Lc2Cer, **c** anti-Gb3Cer, **d** anti-Gb4Cer antibody, and **e** Stx1/anti-Stx1-antibody. Bound antibodies were visualized with alkaline phosphatase conjugated secondary antibodies and BCIP as a substrate. GSL extracts of HBMECs and EA.hy 926 cells were chromatographed together with neutral standard GSLs from human erythrocytes (Std). Applied extracts correspond to 2×10^6 HBMECs and EA.hy 926 cells in **a** and **b** and to 5×10^5 endothelial cells in **c**–**e**. Amounts of standard GSLs were 20 μg in **a** and **e**, 5 μg in **b** and **c**, and 1 μg in **d**. Lc2: Lc2Cer, Gb3: Gb3Cer, Gb4: Gb4Cer. The GSL structures are depicted in Table 1. The *vertical white lines* indicate areas of noncontiguous lanes assembled

rocytes. The initial identification of neutral GSL structures deduced from their chromatographic behaviour (subsequently confirmed by HPTLC immunostaining with specific antibodies) demonstrated the globo-series neutral GSLs Gb3Cer and Gb4Cer as the predominant GSLs in HBMECs, while Lc2Cer and Gb3Cer are the superior GSLs in EA.hy 926 cells. HPTLC-scanning of the prevalent orcinol-stained neutral GSL bands of HBMECs on a percentage level demonstrated an almost equal ratio of Gb3Cer and Gb4Cer (42 and 36%, respectively), and lesser amounts of Lc2Cer (12%) and monohexosylceramide (10%) (Fig. 5a). EA.hy 926 cells showed a substantial relative increase of Gb3Cer (50%) and Lc2Cer (46%), but diminished content of monohexosylceramide (4%) and the lack of Gb4Cer (Fig. 5a). Thus, compared with HBMECs, the overall and most important features of EA.hy 926 cells are their enhanced expression of the Stx1 receptor Gb3Cer and its precursor Lc2Cer, and the obvious absence of Gb4Cer. These tentative structures were further verified by HPTLC immunostaining. The anti-Lc2Cer, anti-Gb3Cer, and anti-Gb4Cer immunostains are shown in Fig. 5b,c, and d, respectively, indicating an approximate 3.4 fold overexpression of Lc2Cer (b) and 2.5-fold overexpression of Gb3Cer (c) in EA.hy 926 cells compared to HBMECs. The absolute amounts of Gb3Cer accounted for 0.23 and 0.62 μg in 1×10^5 HBMECs and EA.hy 926 cells, respectively. Only trace quantities of Gb4Cer are detectable in EA.hy 926 cells (Fig. 5d). The corresponding overlay assay with Stx1 confirmed enhanced expression of Stx1 receptor Gb3Cer in EA.hy 926 cells (Fig. 5e). Thus, the neutral GSL expression determined by HPTLC correlated with the data obtained by the immunofluorescence microscopy, and the Stx1 receptor expression further correlated with the extent of the toxin-mediated cellular injury by a panel of complementary analyses.

Antibodies were used to detect minor neutral GSLs and gangliosides (see Table 1). In both cell lines, only traces of nLc4Cer were detectable, whereas both lines were negative for Gg3Cer and Gg4Cer (data not shown). The major orcinol-detectable gangliosides in the chromatogram below the neutral GSLs were identified as GM3 (prominent in EA.hy 926 cells, Fig. 5a) and GM2 (elevated in HBMECs, Fig. 5a).

Structural characterization of Stx1 receptors by nanoESI Q-TOF-MS

Finally, the Gb3Cer species of the Stx1/anti-Stx1 immunostained HPTLC bands of HBMECs and EA.hy 926 cells (see Fig. 5e) were structurally characterized in detail by nanoESI Q-TOF mass spectrometry. For this purpose, the silica gel of immunopositive bands was scraped off the plate, extracted and the GSLs in the extracts analysed by mass spectrometry. The sodiated molecular ions obtained by nanoESI Q-TOF-MS from the silica gel extracts of Stx1-stained GSLs of HBMECs and EA.hy 926 cells are listed in Table 2. The nanoESI Q-TOF mass spectra and the

Table 2 Major molecular ions identified in the nanoESI Q-TOF mass spectra of Stx1-detected Gb3Cer species from HBMECs and EA.hy 926 cells and their proposed structures

$[M+Na]^+$, *m/z* HBMECs[a]	$[M+Na]^+$, *m/z* EA.hy 926 cells[a]	Proposed structure
1,046.64	1,046.70	Gb3Cer (d18:1, C16:0)
1,130.74	1,130.80	Gb3Cer (d18:1, C22:0)
1,156.76	1,156.78	Gb3Cer (d18:1, C24:1)
1,158.80	1,158.79	Gb3Cer (d18:1, C24:0)

[a] Protonated molecular ions $[M+H]^+$ detectable in the mass spectra of Figs. 6 and 7 are not listed

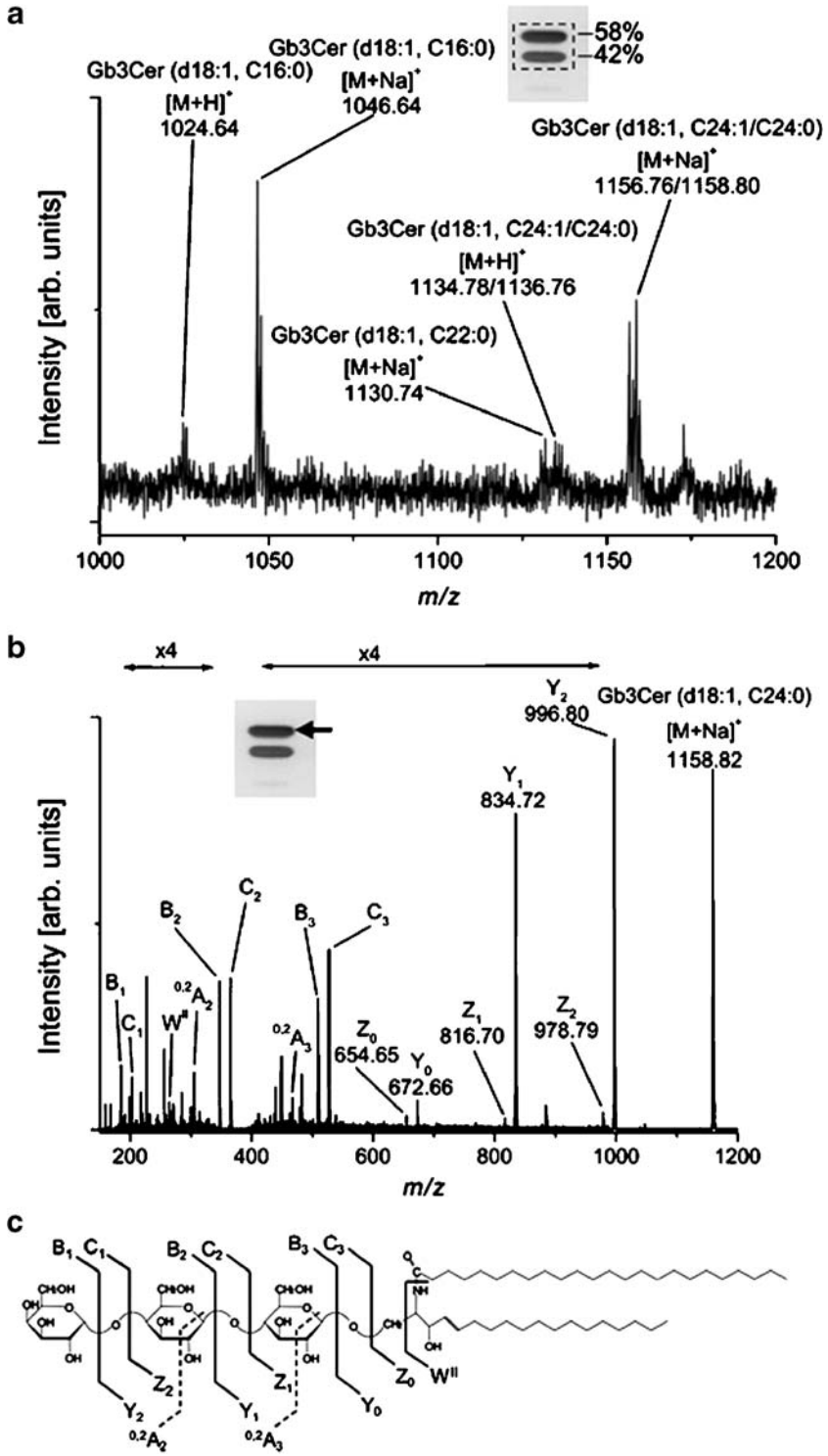

Fig. 6 NanoESI Q-TOF mass spectra of Stx1/anti-Stx1-detected Gb3Cer species from HBMECs. The spectra were obtained from crude HPTLC immunostain-derived silica gel extracts and recorded in the positive ion mode. The corresponding overlay assay is shown in the inset and percentage quotations represent the relative quantities of Stx1-positive upper and lower Gb3Cer bands. **a** Mass spectrum of Gb3Cer (see *dotted rectangle* in the inset). The molecular ions are listed in Table 2. **b** MS/MS spectrum Gb3Cer (d18:1, C24:0) with *m/z* 1158.82. The *arrow* denotes the Gb3Cer precursor ion species selected for CID. Y- and Z-type ions are marked with their corresponding *m/z*-values. **c** Molecular structure and fragmentation scheme of Gb3Cer (d18:1, 24:0). The fragment ions are listed in Table 3

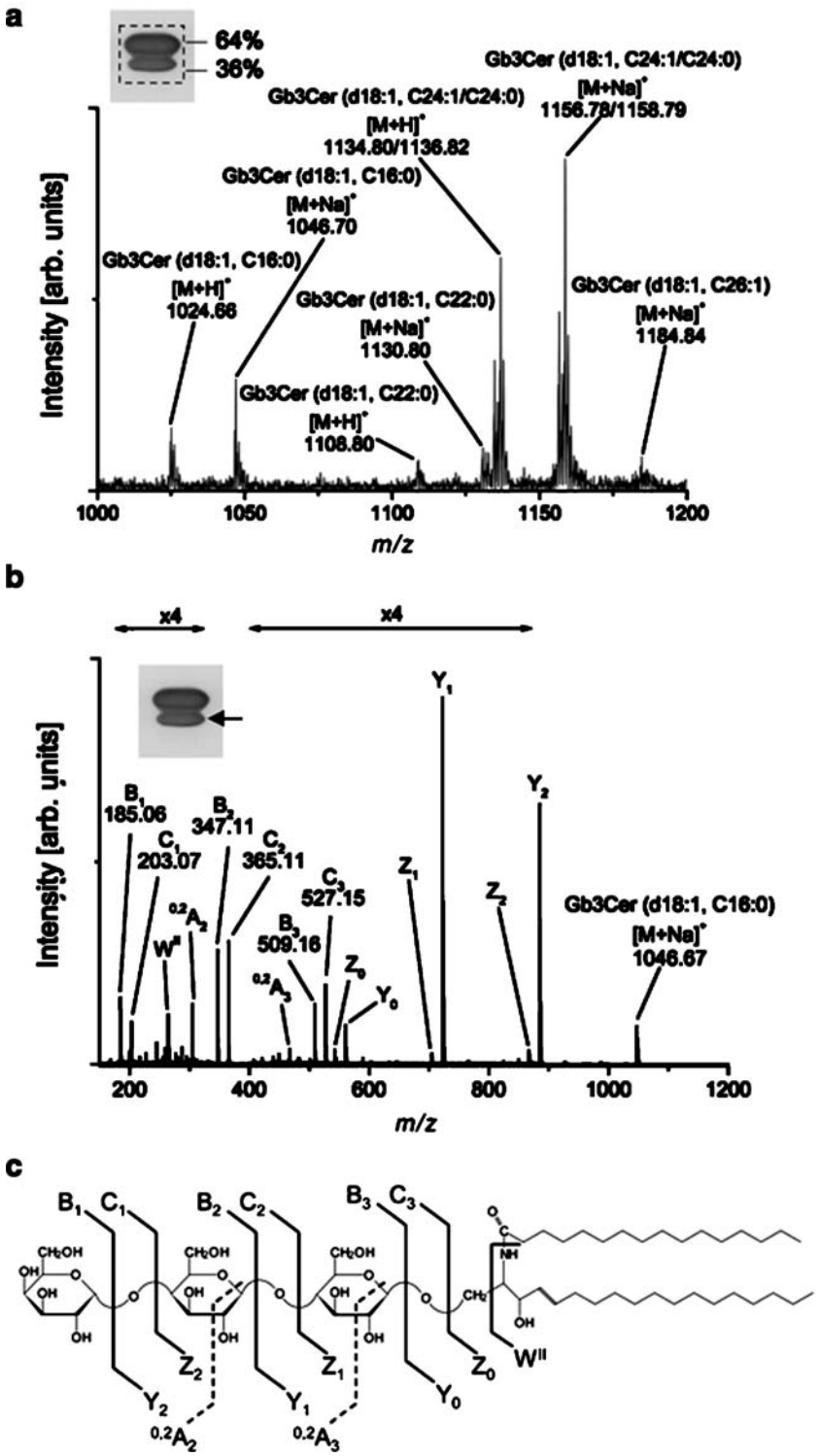

Fig. 7 NanoESI Q-TOF mass spectra of Stx1/anti-Stx1-detected Gb3Cer species from EA.hy 926 cells. The spectra were obtained from crude HPTLC immunostain-derived silica gel extracts and recorded in the positive ion mode. The corresponding overlay assay is shown in the inset and percentage quotations represent the relative quantities of Stx1-positive upper and lower Gb3Cer bands. **a** Mass spectrum of Gb3Cer (see *dotted rectangle* in the inset). The molecular ions are listed in Table 2. **b** MS/MS spectrum of Stx1-detected Gb3Cer (d18:1, C16:0) with *m/z* 1046.67. The *arrow* denotes the Gb3Cer precursor ion species selected for CID. B- and C-type ions are marked with their corresponding *m/z*-values. **c** Molecular structure and fragmentation scheme of Gb3Cer (d18:1, 16:0). The fragment ions are listed in Table 3

Table 3 Type of fragment ions and corresponding *m/z*-values of Stx1-detected major Gb3Cer species in HBMECs and EA.hy 926 cells

	HBMECs		**EA.hy 926 cells**	
	Gb3Cer (d18:1, C16:0) *m/z* 1046.68	Gb3Cer (d18:1, C24:0) *m/z* 1158.82	Gb3Cer (d18:1, C16:0) *m/z* 1046.67	Gb3Cer (d18:1, C24:0) *m/z* 1158.83
Fragment ions	*m/z* values	*m/z* values	*m/z* values	*m/z* values
$^{0,2}A_2$	305.09	305.08	305.09	305.11
$^{0,2}A_3$	467.17	467.15	467.17	467.20
Y_0; Z_0	560.52; 542.48	672.66; 654.65	560.51; 542.50	672.66; 654.66
Y_1; Z_1	722.55; 704.55	834.72; 816.70	722.57; 704.57	834.71; 816.70
Y_2; Z_2	884.62; 866.62	996.80; 978.79	884.61; 866.61	996.78; 978.78
B_1; C_1	185.05; 203.05	185.03; 203.04	185.06; 203.07	185.06; 203.07
B_2; C_2	347.11; 365.11	347.10; 365.11	347.11; 365.11	347.13; 365.13
B_3; C_3	509.17; 527.16	509.15; 527.17	509.16; 527.15	509.19; 527.19
W^{II}	264.28	264.25	264.29	264.30

corresponding insets of Stx1-stained double bands of Gb3Cer from HBMECs and EA.hy 926 cells are shown in Figs. 6a and 7a, respectively. The main species in both spectra correspond to $[M+Na]^+$ molecular ions of Gb3Cer (d18:1, C16:0) and Gb3Cer (d18:1, C24:1/C24:0), accompanied by minor ions of Gb3Cer (d18:1, C22:0). Additionally, the corresponding protonated molecular ions of Gb3Cer (d18:1, 16:0) and Gb3Cer (d18:1, C24:1/C24:0) were detected in both spectra. According to the intensities of immunostained bands, Gb3Cer species with C24:1/C24:0 and C16:0 fatty acids were similarly distributed in HBMECs (58 and 42%, respectively; see Fig. 6a), whereas Gb3Cer variants containing C24:1/C24:0 fatty acids predominated over those with C16:0 fatty acids in EA.hy 926 cells (64 and 36%, respectively; see Fig. 7a).

To finally confirm the identity of Gb3Cer species as Stx1 receptors, the complete structural characterization was exemplified for the main species assigned to Gb3Cer (d18:1, C16:0) and Gb3Cer (d18:1, C24:0) using CID tandem mass spectrometry (Table 3). The MS/MS spectrum of Gb3Cer (d18:1, C24:0) from HBMECs and the corresponding fragmentation scheme are shown in Fig. 6b and c, respectively, and the MS/MS spectrum of Gb3Cer (d18:1, C16:0) from EA.hy 926 cells and the corresponding fragmentation scheme are shown in Fig. 7b and c, respectively. The fragment ions originated from the sodiated precursor ions at *m/z* 1158.82 (Fig. 6b and c) and at *m/z* 1,046.67 (Fig. 7b and c) are assigned according to the nomenclature of Domon and Costello [52, 53]. Full series of Y- and Z-type and B- and C-type ions were obtained, indicating the sequential loss of the three hexose moieties from Gb3Cer. Additionally, the $^{0,2}A_2$- and $^{0,2}A_3$-ions, generated by ring cleavages, and the W^{II}-ions, indicative for the presence of 4-sphingenine (d18:1), give rise to the complete structure of the Stx1 ligands Gb3Cer (Table 3).

Major molecular ions of the silica gel extracts of anti-Gb4Cer positive GSL bands from HBMECs (see Fig. 5d) demonstrated Gb4Cer species with ceramide moieties containing 4-sphingenine (d18:1) and fatty acids with varying fatty acid chain lengths C16:0, C22:0, and C24:1/C24:0 (data not shown). No signals were obtained for Gb4Cer species in EA.hy 926 cells (see Fig. 5d).

Discussion

In the present study we explored the molecular basis of different sensitivities of HBMECs and EA.hy 926 cells to the cytotoxic action of Stx1. Our report is the first detailed comparative analysis showing that the differences in the expression of Stx1-receptors correlate with low and high Stx1-sensitivity of HBMECs and EA.hy 926 cells, respectively. Loss of Gb4Cer synthase resulting in an concomitant accumulation of Gb3Cer renders EA.hy 926 cells an excellent target cell line for Stx1. Despite the fact that HUVEC-derived EA.hy 926 cells exhibit a changed GSL-profile compared to HUVECs, this human cell line represents a superior tool for the investigation of the cytotoxic potential of Stxs and their variants.

The enhanced expression of Stx1-receptor Gb3Cer in EA.hy 926 cells, determined by immunofluorescence microscopy and HPTLC immunodetection, represents the most plausible reason for augmented sensitivity of EA.hy 926 cells. The fine characterization of Gb3Cer species by nanoESI Q-TOF-MS revealed prevalence of Gb3Cer species with C24-fatty acid in EA.hy 926 cells in comparison to HBMECs. According to our current knowledge one may wonder whether these quantitative and qualitative differences in Gb3Cer expression can account

for this important variation. However, the acquisition of receptor details is fundamental to learn more about the membrane architecture required for efficient binding and uptake of the toxin. In addition, we have to gain insights into the lipid and protein environment of the different Gb3Cer species in order to explore the functional role of ceramide variations in the Gb3Cer-mediated intracellular trafficking and delivery of Stx1 to exert its toxic action.

Microvascular endothelial cells from the human brain have been reported to be insensitive to Stx1 and to require incubation with proinflammatory cytokines to overcome this resistance [36–39]. Exposure to cytokines resulted in increased Stx binding and Stx toxicity, which correlated with augmented Gb3Cer content. In our hands, quiescent HBMECs were found to moderately respond without addition of cytokines. Different Stx1 susceptibilities have been reported for various other types of endothelial cells [54–56] and the principal association between the degree of Stx sensitivity and amount of Gb3Cer is generally recognized. Thus, enhanced expression of Gb3Cer appears to be the main reason for the elevated susceptibility of EA.hy 926 cells to Stx1 as compared to HBMECs. The cytotoxicity studies in Fig. 3 suggest that there may be a major Stx1-sensitive and a minor Stx1-resistant population of EA.hy 926 cells. In fact the immunohistochemical detection of Gb3Cer in EA.hy 926 cells (Fig. 2) indicates a low number of Gb3Cer negative cells in the subconfluent culture. The same phenomenon, *i.e.*, a non-homogeneous GSL-expression in pre-confluent cell cultures, has been reported for the immunochemical detection of GM3 in human fibroblasts by Rösner *et al*. [57]. Thus, a cell density- and/or cell cycle-dependent expression could explain the observed faint heterogeneity of Stx1-receptor expression and cytotoxicity response in EA.hy 926 cells.

EA.hy 926 cells have been in culture for many population doublings beyond the level at which primary cells generally succumb to senescence. Because the lifetime of HUVECs is limited and cell properties can change during culture, this perpetual hybrid cell line offers advantages and is commonly used as an equivalent to HUVECs [24, 26, 27, 29]. A detailed previous investigation demonstrated Gb4Cer and Gb3Cer as the most abundant neutral GSLs in HUVECs accounting for 36% and 23% of total neutral GSLs, respectively [33]. The lack of Gb4Cer synthase along with the absence of Gb4Cer in EA.hy 926 cells result in accumulation of Gb3Cer (50% of total neutral GSLs). We thus speculate that the loss of Gb4Cer synthase must have occurred during fusion and/or the following rearrangement of the chromosomes in hybrid EA.hy 926 cells. In any event, the enhanced expression of Gb3Cer changes the HUVEC descendant into a highly Stx1-sensitive cell line, but the truncated GSL pattern is no longer typical of HUVECs.

The fatty acid chain of Gb3Cer influences the binding of Stx [58]. C20:0 and C22:1 fatty acid containing Gb3Cer have the greatest capacity to bind Stx1, and unsaturated [59] or α-hydroxylated fatty acids [60] increased toxin binding. However, neither C20:0 and C22:1 nor hydroxylated fatty acid substituted Gb3Cer species were detectable in HBMECs and EA.hy 926 cells, which excludes their specific involvement in Stx1 binding to these cell types. Our study demonstrates almost equal amounts of long chain C24:1/C24:0 (58%) *versus* short chain C16:0 fatty acids (42%) in Gb3Cer species of HBMECs. The relative content of long chain fatty acids was remarkably increased in EA.hy 926 cells (64%) along with a decrease of short chain fatty acids (36%). Gb3Cer species with saturated C24:0 fatty acid clearly predominated over those with unsaturated C24:1 fatty acids in EA.hy 926 cells, whereas HBMECs showed a balanced ratio of both. In view of these ceramide heterogeneities, any difference between the cell lines might be related to the differences in their susceptibility to Stx1. Gb3Cer species with long chain fatty acids have in fact been suggested being associated with greater toxicity, because they possibly better mediate the localization of internalized toxin to the endoplasmic reticulum [61]. Although the details are unknown, the differences in the overall glycolipid composition of sensitive and resistant cells expressing compositional identical Gb3Cer species may also affect Gb3Cer recognition and the sorting route of incorporated Stx1 as shown for Vero cells [62].

Within the cell membrane, GSLs are clustered as membrane microdomains [63, 64] and function as attachment platforms for host pathogens and their toxins [65]. Only GSLs that associate strongly with detergent-resistant membrane microdomains appear to carry AB_5 toxins from the plasma membrane to the endoplasmic reticulum in a retrograde fashion [66]. The association of Gb3Cer with microdomains is required in HeLa cells for the retrograde transport of Stx B-subunit [67]. Glucosylceramide has been identified as a modulator of Stx-microdomain association and as an essential requirement in the endoplasmic reticulum for a cytotoxic effect [68], and functionally different pools of Gb3Cer have been proposed to underlie the cellular dynamics of Stx-mediated recruitment to microdomains in HeLa cells [69]. Although the exact roles of the ceramide heterogeneity of Gb3Cer and the involvement of auxiliary glycolipids in Stx-mediated damage of endothelial and many other cells remain to be elucidated, we hypothesize a functional role of certain Gb3Cer species that might provide a molecular basis for the different Stx1-susceptibility of various cell types.

Infections caused by Stx-producing *Escherichia coli* result in a spectrum of outcomes ranging from asymptomatic carriage to uncomplicated diarrhea, bloody diarrhea, and the hemolytic uremic syndrome [2, 70]. Thus, an

increasing knowledge about the molecular details of Stx-receptors and their assembly in the plasma membrane is important to better understand the pathways of intracellular transport of Stx [66] and to develop preventive and therapeutic measures for Stx-mediated diseases [71].

Acknowledgements This work was supported by grants from the Deutsche Forschungsgemeinschaft (DFG), program "Infections of the Endothelium" SPP 1130 project KA 717/4-2 (H.K.), the SFB 629 (B2, M.A.S.), the cooperative projects FR2569/1-1 (A.W.F.) and MU845/4-1 (J.M.) and a grant from the Interdisciplinary Center of Clinical Research (IZKF) Münster, project no. Ka2/061/04 (H.K.).

The authors gratefully acknowledge the expert technical assistance of M. Hülsmann, E. Kalthoff, and L. Greune. We thank Phillip I. Tarr (Washington University School of Medicine, St. Louis, MO, USA) for critical reading of the manuscript and stimulating discussions.

References

1. Sandvig, K.: Shiga toxins. Toxicon. **39**, 1629–1635 (2001)
2. Karch, H., Tarr, P.I., Bielaszewska, M.: Enterohaemorrhagic *Escherichia coli* in human medicine. Int. J. Med. Microbiol. **295**, 405–418 (2005)
3. Ling, H., Boodhoo, A., Hazes, B., Cummings, M.D., Armstrong, G.D., Brunton, J.L., Read, R.J.: Structure of the Shiga-like toxin I B-pentamer complexed with an analogue of its receptor Gb_3. Biochemistry **37**, 1777–1788 (1998)
4. Lingwood, C.A.: Role of verotoxin receptors in pathogenesis. Trends Microbiol. **4**, 147–153 (1996)
5. Sandvig, K., Garred, Ø., Prydz, K., Kozlov, J.V., Hansen, S.H., van Deurs, B.: Retrograde transport of endocytosed Shiga toxin to the endoplasmic reticulum. Nature **358**, 510–512 (1992)
6. Endo, Y., Tsurugi, K., Yutsudo, T., Takeda, Y., Ogasawara, T., Igarashi, K.: Site of action of a Vero toxin (VT2) from *Escherichia coli* O157:H7 and Shiga toxin on eukaryotic ribosomes. Eur. J. Biochem. **171**, 45–50 (1988)
7. Garred, Ø., van Deurs, B., Sandvig, K.: Furin-induced cleavage and activation of Shiga toxin. J. Biol. Chem. **270**, 10817–10821 (1995)
8. Stults, C.L., Sweeley, C.C., Macher, B.A.: Glycosphingolipids: structure, biological source, and properties. Methods Enzymol. **179**, 167–214 (1989)
9. Müthing, J.: Mammalian glycosphingolipids. In: Freiser-Reid, B., Tatsuka, K., Thiem, J. (eds.) Glycoscience: Chemistry and Chemical Biology, vol. 3, pp. 2220–2249. Springer-Verlag, Heidelberg, Germany (2001)
10. Schnaar, R.L.: Glycosphingolipids in cell surface recognition. Glycobiology **1**, 477–485 (1991)
11. Feizi, T.: Carbohydrate-mediated recognition systems in innate immunity. Immunol. Rev. **173**, 79–88 (2000)
12. Schlossmacher, M.G., Cullen, V., Müthing, J.: The glucocerebrosidase gene and Parkinson's disease in Ashkenazi Jews. N. Engl. J. Med. **352**, 728–731 (2005)
13. Karlsson, K.A.: Animal glycosphingolipids as membrane attachment sites for bacteria. Annu. Rev. Biochem. **58**, 309–350 (1989)
14. Teneberg, S., Ångström, J., Ljungh, Å.: Carbohydrate recognition by enterohemorrhagic *Escherichia coli*: characterization of a novel glycosphingolipid from cat small intestine. Glycobiology. **14**, 187–196 (2004)
15. Miller-Podraza, H., Lanne, B., Ångström, J., Teneberg, S., Milh, M.A., Jovall, P.Å., Karlsson, H., Karlsson, K.A.: Novel binding epitope for *Helicobacter pylori* found in neolacto carbohydrate chains: structure and cross-binding properties. J. Biol. Chem. **280**, 19695–19703 (2005)
16. Nakamura, K., Suzuki, M., Inagaki, F., Yamakawa, T., Suzuki, A.: A new ganglioside showing choleragenoid-binding activity in mouse spleen. J. Biochem. **101**, 825–835 (1987)
17. Stins, M.F., Gilles, F., Kim, K.S.: Selective expression of adhesion molecules on human brain microvascular endothelial cells. J. Neuroimmunol. **76**, 81–90 (1997)
18. Edgell, C.J.S., McDonald, C.C., Graham, J.B.: Permanent cell line expressing human factor VIII-related antigen established by hybridization. Proc. Natl. Acad. Sci. U.S.A. **80**, 3734–3737 (1983)
19. Kim, K.S.: Pathogenesis of bacterial meningitis: from bacteraemia to neuronal injury. Nat. Rev. Neurosci. **4**, 376–385 (2003)
20. Bielaszewska, M., Karch, H.: Consequences of enterohaemorrhagic *Escherichia coli* infection for the vascular endothelium. Thromb. Haemost. **94**, 312–318 (2005)
21. Kim, K.J., Chung, J.W., Kim, K.S.: 67-kDa laminin receptor promotes internalization of cytotoxic necrotizing factor 1-expressing *Escherichia coli* K1 into human brain microvascular endothelial cells. J. Biol. Chem. **280**, 1360–1368 (2005)
22. Shin, S., Kim, K.S.: RhoA and Rac1 contribute to type III group B streptococcal invasion of human brain microvascular endothelial cells. Biochem. Biophys. Res. Commun. **345**, 538–542 (2006)
23. Khan, N.A., Kim, Y., Shin, S., Kim, K.S.: FimH-mediated *Escherichia coli* K1 invasion of human brain microvascular endothelial cells. Cell. Microbiol. **9**, 169–178 (2007)
24. Bielaszewska, M., Sinha, B., Kuczius, T., Karch, H.: Cytolethal distending toxin from Shiga toxin-producing *Escherichia coli* O157 causes irreversible G_2/M arrest, inhibition of proliferation, and death of human endothelial cells. Infect. Immun. **73**, 552–562 (2005)
25. Kügler, S., Böcker, K., Heusipp, G., Greune, L., Kim, K.S., Schmidt, M.A.: Pertussis toxin transiently affects barrier integrity, organelle organization and transmigration of monocytes in a human brain microvascular endothelial cell barrier model. Cell. Microbiol. **9**, 619–632 (2007)
26. Emeis, J.J., Edgell, C.J.S.: Fibrinolytic properties of a human endothelial hybrid cell line (Ea.hy 926). Blood **71**, 1669–1675 (1988)
27. Schönherr, E., Schaefer, L., O'Connell, B.C., Kresse, H.: Matrix metalloproteinase expression by endothelial cells in collagen lattices changes during co-culture with fibroblasts and upon induction of decorin expression. J. Cell. Physiol. **187**, 37–47 (2001)
28. Strazynski, M., Eble, J.A., Kresse, H., Schönherr, E.: Interleukin (IL)-6 and IL-10 induce decorin mRNA in endothelial cells, but interaction with fibrillar collagen is essential for its translocation. J. Biol. Chem. **279**, 21266–21270 (2004)
29. Kainulainen, V., Nelimarkka, L., Järveläinen, H., Laato, M., Jalkanen, M., Elenius, K.: Suppression of syndecan-1 expression in endothelial cells by tumor necrosis factor-α. J. Biol. Chem. **271**, 18759–18766 (1996)
30. Obrig, T.O., Del Vecchio, P.J., Brown, J.E., Moran, T.P., Rowland, B.M., Judge, T.K., Rothman, S.W.: Direct cytotoxic action of Shiga toxin on human vascular endothelial cells. Infect. Immun. **56**, 2373–2378 (1988)
31. Kaye, S.A., Louise, C.B., Boyd, B., Lingwood, C.A., Obrig, T.G.: Shiga toxin-associated hemolytic uremic syndrome: interleukin-1β enhancement of Shiga toxin cytotoxicity toward human vascular endothelial cells in vitro. Infect. Immun. **61**, 3886–3891 (1993)
32. Gillard, B.K., Jones, M.A., Marcus, D.M.: Glycosphingolipids of human umbilical vein endothelial cells and smooth muscle cells. Arch. Biochem. Biophys. **256**, 435–445 (1987)
33. Müthing, J., Duvar, S., Heitmann, D., Hanisch, F.G., Neumann, U., Lochnit, G., Geyer, R., Peter-Katalinić, J.: Isolation and structural characterization of glycosphingolipids of *in vitro*

propagated human umbilical vein endothelial cells. Glycobiology **9**, 459–468 (1999)
34. Kanda, T., Ariga, T., Kubodera, H., Jin, H.L., Owada, K., Kasama, T., Yamawaki, M., Mizusawa, H.: Glycosphingolipid composition of primary cultured human brain microvascular endothelial cells. J. Neurosci. Res. **78**, 141–150 (2004)
35. Van de Kar, N.C.A.J., Monnens, L.A.H., Karmali, M.A., van Hinsbergh, V.W.M.: Tumor necrosis factor and interleukin-1 induce expression of the verocytotoxin receptor globotriaosylceramide on human endothelial cells: implications for the pathogenesis of the hemolytic uremic syndrome. Blood **80**, 2755–2764 (1992)
36. Ramegowda, B., Samuel, J.E., Tesh, V.L.: Interaction of Shiga toxins with human brain microvascular endothelial cells: cytokines as sensitizing agents. J. Infect. Dis. **180**, 1205–1213 (1999)
37. Eisenhauer, P.E., Chaturvedi, P., Fine, R.E., Ritchie, A.J., Pober, J.S., Cleary, T.G., Newburg, D.S.: Tumor necrosis factor alpha increases human cerebral endothelial cell Gb_3 and sensitivity to Shiga toxin. Infect. Immun. **69**, 1889–1894 (2001)
38. Stricklett, P.K., Hughes, A.K., Ergonul, Z., Kohan, D.E.: Molecular basis for up-regulation by inflammatory cytokines of Shiga toxin 1 cytotoxicity and globotriaosylceramide expression. J. Infect. Dis. **186**, 976–982 (2002)
39. Ergonul, Z., Hughes, A.K., Kohan, D.E.: Induction of apoptosis of human brain microvascular endothelial cells by Shiga toxin. J. Infect. Dis. **187**, 154–158 (2003)
40. Duvar, S., Peter-Katalinić, J., Hanisch, F.G., Müthing, J.: Isolation and structural characterization of glycosphingolipids of *in vitro* propagated bovine aortic endothelial cells. Glycobiology **7**, 1099–1109 (1997)
41. Heidemann, R., Riese, U., Lütkemeyer, D., Büntemeyer, H., Lehmann, J.: The Super-Spinner: a low cost animal cell culture bioreactor for the CO_2 incubator. Cytotechnology **14**, 1–9 (1994)
42. Meisen, I., Friedrich, A.W., Karch, H., Witting, U., Peter-Katalinić, J., Müthing, J.: Application of combined high-performance thin-layer chromatography immunostaining and nanoelectrospray ionisation quadrupole time-of-flight tandem mass spectrometry to the structural characterization of high- and low-affinity binding ligands of Shiga toxin 1. Rapid Commun. Mass Spectrom. **19**, 3659–3665 (2005)
43. Kasai, M., Iwamori, M., Nagai, Y., Okumura, K., Tada, T.: A glycolipid on the surface of mouse natural killer cells. Eur. J. Immunol. **10**, 175–180 (1980)
44. Müthing, J., Burg, M., Möckel, B., Langer, M., Metelmann-Strupat, W., Werner, A., Neumann, U., Peter-Katalinić, J., Eck, J.: Preferential binding of the anticancer drug rViscumin (recombinant mistletoe lectin) to terminally α2-6-sialylated neolacto-series gangliosides. Glycobiology **12**, 485–497 (2002)
45. Müthing, J., Meisen, I., Kniep, B., Haier, J., Senninger, N., Neumann, U., Langer, M., Witthohn, K., Milosević, J., Peter-Katalinić, J.: Tumor-associated CD75s gangliosides and CD75s-bearing glycoproteins with Neu5Acα2-6Galβ1-4GlcNAc residues are receptors for the anticancer drug rViscumin. FASEB J. **19**, 103–105 (2005)
46. Steffensen, R., Carlier, K., Wiels, J., Levery, S.B., Stroud, M., Cedergren, B., Sojka, B.N., Bennett, E.P., Jersild, C., Clausen, H.: Cloning and expression of the histo-blood group P^k UDP-galactose: Galβ1-4Glcβ1-1Cer α1,4-galactosyltransferase. J. Biol. Chem. **275**, 16723–16729 (2000)
47. Müthing, J., Meisen, I., Bulau, P., Langer, M., Witthohn, K., Lentzen, H., Neumann, U., Peter-Katalinić, J.: Mistletoe lectin I is a sialic acid-specific lectin with strict preference to gangliosides and glycoproteins with terminal Neu5Acα2-6Galβ1-4GlcNAc residues. Biochemistry **43**, 2996–3007 (2004)
48. Müthing, J., Unland, F., Heitmann, D., Orlich, M., Hanisch, F.G., Peter-Katalinić, J., Knäuper, V., Tschesche, H., Kelm, S., Schauer, R., Lehmann, J.: Different binding capacities of influenza A and Sendai viruses to gangliosides from human granulocytes. Glycoconj. J. **10**, 120–126 (1993)
49. Müthing, J.: TLC in structure and recognition studies of glycosphingolipids. In: Hounsell, E.F. (ed.) Methods in Molecular Biology, pp. 183–195. Humana, Totawa, NJ (1998)
50. Meisen, I., Peter-Katalinić, J., Müthing, J.: Direct analysis of silica gel extracts from immunostained glycosphingolipids by nano-electrospray ionization quadrupole time-of-flight mass spectrometry. Anal. Chem. **76**, 2248–2255 (2004)
51. Meisen, I., Peter-Katalinić, J., Müthing, J.: Discrimination of neolacto-series gangliosides with α2-3- and α2-6-linked *N*-acetylneuraminic acid by nanoelectrospray ionization low-energy collision-induced dissociation tandem quadrupole TOF MS. Anal. Chem. **75**, 5719–5725 (2003)
52. Domon, B., Costello, C.E.: A systematic nomenclature for carbohydrate fragmentations in FAB-MS/MS spectra of glycoconjugates. Glycoconj. J. **5**, 397–409 (1988)
53. Domon, B., Costello, C.E.: Structure elucidation of glycosphingolipids and gangliosides using high-performance tandem mass spectrometry. Biochemistry **27**, 1534–1543 (1988)
54. Obrig, T.G., Louise, C.B., Lingwood, C.A., Boyd, B., Barley-Maloney, L., Daniel, T.O.: Endothelial heterogeneity in Shiga toxin receptors and responses. J. Biol. Chem. **268**, 15484–15488 (1993)
55. Ohmi, K., Kiyokawa, N., Takeda, T., Fujimoto, J.: Human microvascular endothelial cells are strongly sensitive to Shiga toxins. Biochem. Biophys. Res. Commun. **251**, 137–141 (1998)
56. Jacewicz, M., Acheson, D.W.K., Binion, D.G., West, G.A., Lincicome, L.L., Fiocchi, C., Keusch, G.T.: Responses of human intestinal microvascular endothelial cells to Shiga toxins 1 and 2 and pathogenesis of hemorrhagic colitis. Infect. Immun. **67**, 1439–1444 (1999)
57. Rösner, H., Greis, Ch., Rodemann, H.P.: Density-dependent expression of ganglioside GM3 by human skin fibroblasts in an all-or-none fashion, as a possible modulator of cell growth *in vitro*. Exp. Cell Res. **190**, 161–169 (1990)
58. Boyd, B., Magnusson, G., Zhiuyan, Z., Lingwood, C.A.: Lipid modulation of glycolipid receptor function. Eur. J. Biochem. **223**, 873–878 (1994)
59. Kiarash, A., Boyd, B., Lingwood, C.A.: Glycosphingolipid receptor function is modified by fatty acid content. J. Biol. Chem. **269,** 11138–11146 (1994)
60. Binnington, B., Lingwood, D., Nutikka, A., Lingwood, C.A.: Effect of globotriaosylceramide fatty acid α-hydroxylation on the binding by verotoxin 1 and verotoxin 2. Neurochem. Res. **27**, 807–813 (2002)
61. Sandvig, K., Ryd, M., Garred, Ø., Schweda, E., Holm, P.K., van Deurs, B.: Retrograde transport from the Golgi complex to the ER of both Shiga toxin and the nontoxic Shiga B-fragment is regulated by butyric acid and cAMP. J. Cell Biol. **126**, 53–64 (1994)
62. Sekino, T., Kiyokawa, N., Taguchi, T., Takenouchi, H., Matsui, J., Tang, W.R., Suzuki, T., Nakajima, H., Saito, M., Ohmi, K., Katagiri, Y.U., Okita, H., Nakao, H., Takeda, T., Fujimoto, J.: Characterization of a Shiga-toxin 1-resistant stock of Vero cells. Microbiol. Immunol. **48**, 377–387 (2004)
63. Hakomori, S.I.: Cell adhesion/recognition and signal transduction through glycosphingolipid microdomain. Glycoconj. J. **17**, 143–151 (2000)
64. Sonnino, S., Prinetti, A., Mauri, L., Chigorno, V., Tettamanti, G.: Dynamic and structural properties of sphingolipids as driving forces for the formation of membrane domains. Chem. Rev. **106**, 2111–2125 (2006)
65. Fantini, J., Maresca, M., Hammache, D., Yahi, N., Delézay, O.: Glycosphingolipid (GSL) microdomains as attachment platforms for host pathogens and their toxins on intestinal epithelial cells:

activation of signal transduction pathways and perturbations of intestinal absorption and secretion. Glycoconj. J. **17**, 173–179 (2000)
66. Lencer, W.I., Saslowsky, D.: Raft trafficking of AB_5 subunit bacterial toxins. Biochim. Biophys. Acta **1746**, 314–321 (2005)
67. Falguières, T., Mallard, F., Baron, C., Hanau, D., Lingwood, C., Goud, B., Salamero, J., Johannes, L.: Targeting of Shiga toxin B-subunit to retrograde transport route in association with detergent-resistant membranes. Mol. Biol. Cell **12**, 2453–2468 (2001)
68. Smith, D.C., Sillence, D.J., Falguières, T., Jarvis, R.M., Johannes, L., Lord, J.M., Platt, F.M., Roberts, L.M.: The association of Shiga-like toxin with detergent-resistant membranes is modulated by glucosylceramide and is an essential requirement in the endoplasmic reticulum for a cytotoxic effect. Mol. Biol. Cell **17**, 1375–1387 (2006)
69. Falguières, T., Römer, W., Amessou, M., Afonso, C., Wolf, C., Tabet, J.C., Lamaze, C., Johannes, L.: Functionally different pools of Shiga toxin receptor, globotriaosyl ceramide, in HeLa cells. FEBS J. **273**, 5205–5218 (2006)
70. Tarr, P.I., Gordon, C.A., Chandler, W.L.: Shiga-toxin-producing *Escherichia coli* and haemolytic uraemic syndrome. Lancet **365**, 1073–1086 (2005)
71. Karmali, M.A.: Prospects for preventing serious systemic toxemic complications of Shiga toxin producing *Escherichia coli* infections using Shiga toxin receptor analogues. J. Infect. Dis. **189**, 355–359 (2004)
72. Müthing, J., Čačić, M.: Glycosphingolipid expression in human skeletal and heart muscle assessed by immunostaining thin-layer chromatography. Glycoconj. J. **14**, 19–28 (1997)
73. Bethke, U., Müthing, J., Schauder, B., Conradt, P., Mühlradt, P. F.: An improved semi-quantitative enzyme immunostaining procedure for glycosphingolipid antigens on high performance thin layer chromatograms. J. Immunol. Methods **89**, 111–116 (1986)
74. Markotić, A., Čulić, V., Kurir, T., Meisen, I., Büntemeyer, H., Boraska, V., Zemunik, T., Petri, N., Mesarić, M., Peter-Katalinić, J., Müthing, J.: Oxygenation alters ganglioside expression in rat liver following partial hepatectomy. Biochem. Biophys. Res. Commun. **330**, 131–141 (2005)
75. Chester, M.A.: IUPAC-IUB Joint Commission on Biochemical Nomenclature. Nomenclature of glycolipids. Recommendations 1997. Glycoconj. J. **16**, 1–6 (1999)